THE JOURNAL OF BIOLOGICAL CHEMISTRY
Vol. 278, No. 40, Issue of October 3, pp. 39185–39188, 2003
Printed in U.S.A.

The NMR Structure of the Sensory Domain of the Membranous Two-component Fumarate Sensor (Histidine Protein Kinase) DcuS of *Escherichia coli**

Received for publication, July 30, 2003, and in revised form, August 7, 2003
Published, JBC Papers in Press, August 7, 2003, DOI 10.1074/jbc.C300344200

Lucia Pappalardo‡, Ingo G. Janausch§, Vinesh Vijayan‡, Eva Zientz§, Jochen Junker‡, Wolfgang Peti‡, Markus Zweckstetter‡, Gottfried Unden§, and Christian Griesinger‡¶

From the ‡Max Planck Institut für Biophysikalische Chemie, Am Fassberg 11, D-37077 Göttingen, Germany and the §Institut für Mikrobiologie und Weinforschung, Universität Mainz, Becherweg 15, D-55099 Mainz, Germany

The structure of the water-soluble, periplasmic domain of the fumarate sensor DcuS (DcuS-pd) has been determined by NMR spectroscopy in solution. DcuS is a prototype for a sensory histidine kinase with transmembrane signal transfer. DcuS belongs to the CitA family of sensors that are specific for sensing di- and tricarboxylates. The periplasmic domain is folded autonomously and shows helices at the N and the C terminus, suggesting direct linking or connection to helices in the two transmembrane regions. The structure constitutes a novel fold. The nearest structural neighbor is the Per-Arnt-Sim domain of the photoactive yellow protein that binds small molecules covalently. Residues Arg^{107}, His^{110}, and Arg^{147} are essential for fumarate sensing and are found clustered together. The structure constitutes the first periplasmic domain of a two component sensory system and is distinctly different from the aspartate sensory domain of the Tar chemotaxis sensor.

The fumarate sensor DcuS is a prototype for a two component sensory histidine kinase with signal perception in the periplasm, transmembrane signal transfer (1, 2), and autophosphorylation of a His residue in the kinase domain in the cytoplasm (3). DcuS belongs to the CitA family of sensors that are specific for sensing di- and tricarboxylates (1, 2, 4, 5). The periplasmic domain of the histidine autokinase CitA works as a highly specific citrate receptor, whereas DcuS uses any type of C_4-dicarboxylate, like fumarate, succinate, and malate, as a stimulus (1, 4–6). DcuS is predicted to consist of two transmenbrane helices and of a periplasmic sensory domain enclosed by the transmembrane helices. The second transmembrane helix is followed by a cytoplasmic PAS[1] domain of unknown function and the kinase with the consensus histidine residue for autophosphorylation. The periplasmic citrate binding domain of CitA is conserved in DcuS and presumably responsible for binding of fumarate and other C_4-dicarboxylates. Preliminary results suggest that fumarate sensing occurs by this domain in the periplasm (2, 4, 5). After phosphorylation by DcuS the response regulator DcuR of the DcuSR system activates the expression of the target genes like *dcuB* and *frdABCD* encoding an anaerobic fumarate carrier DcuB and fumarate reductase (4, 5). Despite their prevalence no structural information is available for transmembranous sensory kinases, in particular not for signal perception and transmission across the membrane. Only the structures of cytoplasmic sensory kinases, or of domains not involved in transmembrane signaling, have been determined.

Purified DcuS is active after reconstitution in proteoliposomes and capable of transmembranous stimulation of the kinase by fumarate (2). For a more detailed understanding of signal perception representing the first step of signal transduction in transmembranous histidine kinases of two-component systems, the structure of the periplasmic C_4-dicarboxylate binding domain of DcuS (DcuS-pd) was determined after stable over-production of the domain.

EXPERIMENTAL PROCEDURES

Overproduction of DcuS$_{45–180}$ ("DcuS-pd")—The sequence of *dcuS* coding for the periplasmic domain of DcuS (DcuS$_{45–180}$ or DcuS-pd) enclosed by the two transmembrane helices was cloned into the *Nde*I and *Hin*dIII sites of plasmid pET28a (Novagen) resulting in plasmid pMW145. The DNA fragment was amplified with oligonucleotides pdcus-*Nde*II (ATT TAC TTC TCG CAT ATG AGT GAT ATG) and pdcuS-Hind (GAC CAG ATA AAG CTT CAG CGA CTG) by PCR of genomic *Escherichia coli* K-12 AN387 DNA. The cloned fragment codes for DcuS-pd starting with Ser^{45} and ending with Arg^{180}. The N-terminal extension contains in addition a His$_6$ tag followed by a thrombin cleavage site in front of DcuS-pd. Overproduction of His6-DcuS-pd was performed in *E. coli* BL21DE3(pMW145) grown aerobically in LB broth or supplemented M9 medium containing [^{13}C]glucose (6 mM) and/or [^{15}N]NH_4Cl (7 mM) as suitable, after induction with 1 mM isopropyl-α-D-thiogalactopyranoside. The washed cells (1.2 g) were broken by two passages through a French press. The soluble protein fraction was used for isolation of His$_6$-DcuS-pd on a column of Ni^{2+}-NTA-agarose (3 ml bed volume). His$_6$-DcuS-pd was eluted in 6–9 ml of buffer containing 500 mM imidazole in 50 mM sodium/potassium phosphate buffer and 200 mM NaCl at pH 7.0.

Sample Preparation for NMR—Isolated His$_6$-DcuS-pd (10–20 mg) was dialyzed (molecular weight 10,000, ZelluTrans, Roth) for 3 h against 100 volumes of buffer containing 5 mM imidazole and 200 mM NaCl in 50 mM sodium/potassium phosphate at pH 6.5. The sample (6 ml) was then concentrated by centrifugation at max. 5000 × *g* in a Vivaspin concentrator tube (exclusion limit 10,000, Vivaspin, Sartorius) to a final concentration of 10–25 mg of protein/ml. The sample (300–900 μl, in fractions of 300 μl each) was frozen in liquid N_2 and stored at −80 °C. For the NMR measurement the His$_6$ tag was removed by incubation of 300-μl samples with thrombin (20 units/mg DcuS)

* This work was supported by the Max Planck Gesellschaft, the Deutsche Forschungsgemeinschaft (UN 49/8-1,2 (to G. U.), GR 1211/12-1,2 (to C. G.), and ZW 71/1-3 (to M. Z.)), and the Fonds der Chemischen Industrie (to C. G. and G. U. and a Kekulé stipend to W. P.). The costs of publication of this article were defrayed in part by the payment of page charges. This article must therefore be hereby marked "*advertisement*" in accordance with 18 U.S.C. Section 1734 solely to indicate this fact.

The atomic coordinates and structure factors (code 1ojg) have been deposited in the Protein Data Bank, Research Collaboratory for Structural Bioinformatics, Rutgers University, New Brunswick, NJ (http://www.rcsb.org/).

¶ To whom correspondence should be addressed. Tel.: 49-551-201-2201; Fax: 49-551-201-2202; E-mail: cigr@nmr.mpibpc.mpg.de.

[1] The abbreviations used are: PAS, Per-Arnt-Sim domain; NOE, nuclear Overhauser effect; NOESY, NOE spectroscopy; HSQC, heteronuclear single quantum coherence; r.m.s.d., root mean square deviation; PYP, photoactive yellow protein.

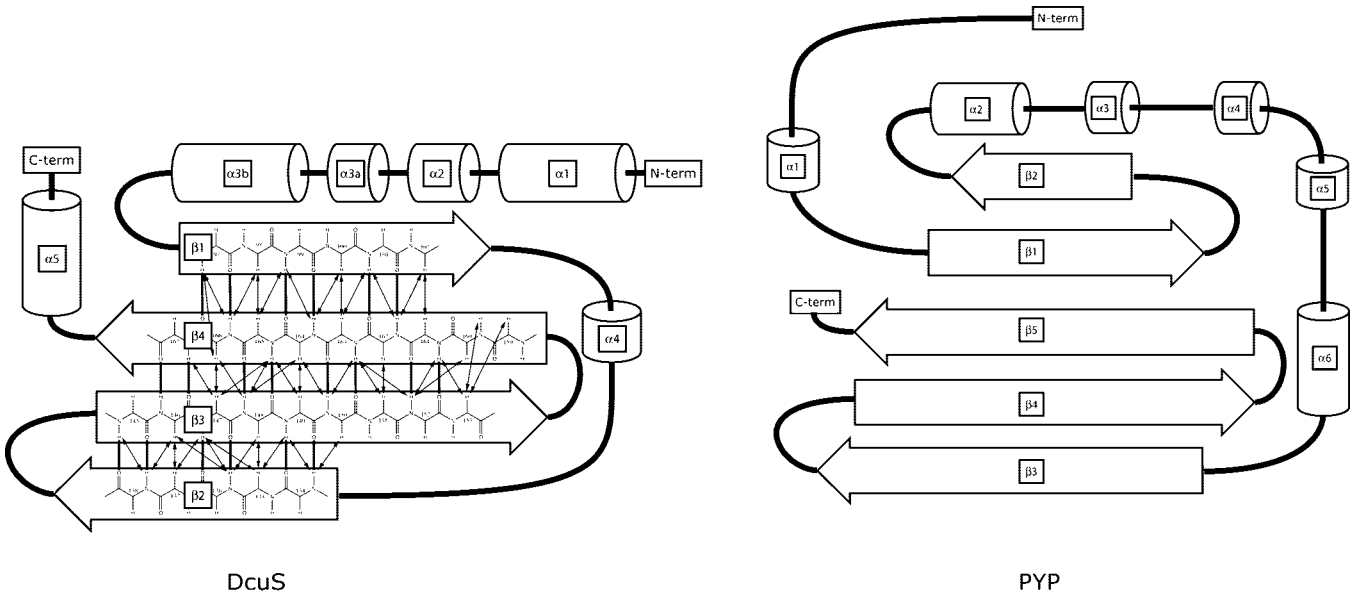

FIG. 1. *Left*, secondary structure of DcuS together with the intrastrand NOEs from which the topology of the β-strands is derived. *Right*, secondary structure of PYP.

(Amersham Biosciences) in 700 μl of buffer for 1 h at 20 °C. The digested sample was passed through a Ni^{2+}-NTA column to remove the His_6 tag. The eluate (6–9 ml) was concentrated in a Vivaspin concentrator tube as described above. Overall 3–7.5 mg of periplasmic domain of DcuS-pd with a Gly-Ser-His-Met extension at the N-terminal end in front of Ser^{45} of DcuS was obtained in 300 μl of buffer. When required, for complete exchange of H_2O against D_2O (99.9%, Deutero GmbH, Kastellaun, Germany), the protein solution was frozen in liquid N_2, freeze-dried for 45 min, and resuspended in 1 ml D_2O followed by lyophilization as described for 3 cycles. The last suspension was kept for 1 h at 4 °C and freeze-dried. The dry sample was dissolved at a final concentration of 30 mg of protein/ml of D_2O, and stored at −80 °C till use.

Assignment—The assignment of His-tagged DcuS-pd has been published previously (7); it was put into BRMB (BioMagResBank) under the accession number 4821. The assignment of DcuS-pd without the His tag differs only slightly from the one with the His tag.

Restraints—Distance restraints were obtained from the intensities of NOE cross-peaks extracted from ^{15}N-edited three-dimensional NOESY-HSQC, two-dimensional NOESY, and ^{13}C-edited three-dimensional NOESY-HSQC spectra. Analysis, assignment and integration of NOESY spectra were accomplished with XEASY (8). NOEs were classified as *strong*, *medium*, *weak*, and *very weak* with an upper distance restraint of 3.0, 3.8, 4.6, and 5.4 Å, respectively. No lower distance limit was applied during initial runs. The lower limit was restrained to 2 Å at a later stage of the calculations. Hydrogen bond restraints were applied in a standard way to slowly exchanging amide protons involved in α-helix and antiparallel β-sheet structures.

Restraints for $(\phi,\psi) = (-57 \pm 20, -47 \pm 20)$ and $(\phi,\psi) = (-139 \pm 20, 135 \pm 20)$ were applied to the amino acid residues involved in α-helix and antiparallel β-sheet secondary structures, respectively, as determined by NOE patterns and TALOS prediction using ^{13}C chemical shifts (9) for non-regular secundary structure elements.

A set of $^1D_{NH}$, $^1D_{NC'}$, $^1D_{C'C\alpha}$, and $^1D_{C\alpha H\alpha}$ residual dipolar couplings of DcuS were calculated from the difference in the corresponding *J* splitting measured in protein sample containing 10 mg/ml Pf1 filamentous phage (10)[2] and in protein sample in the absence of phage (12). $^1D_{NH}$ and $^1D_{NC'}$ residual dipolar couplings were measured simultaneously using a modified interleaved three-dimensional TROSY-HNCO experiment (13) and $^1D_{C\alpha H\alpha}$ and $^1D_{C'C\alpha}$ residual dipolar couplings using a modified interleaved three-dimensional CBCACONH experiment (14). The data sets were processed and analyzed using the NMRPipe/NMRDraw (15) software package. The magnitude of the alignment tensor (Da) obtained from the histogram of measured dipolar couplings is 10.7 Hz for $^1D_{NH}$ and the corresponding rhombicity (*R*) is 0.63. Dipolar couplings were applied in the structure calculation with different weight factors 1.0 ($^1D_{NH}$), 0.4 ($^1D_{C\alpha H\alpha}$), 44 ($^1D_{NC'}$), and 2.5 ($^1D_{C'C\alpha}$).

[2] Asla Laboratories (orion.imm.ki.se/asla/asla-phage.html).

Structure Calculation and Analysis—Structures were calculated using the Xplor-NIH program package (16). A standard four-stage molecular dynamics protocol was used with an initial high temperature annealing stage (1000 step/15-ps torsion angle molecular dynamics at $T = 50{,}000$), followed by a first (1000 step/15-ps cooling to 0) and a second (3000 step/15-ps Cartesian molecular dynamics cooling from $T = 2000$ to 0) slow-cool annealing stage and a final minimization stage. The final structures were analyzed by the programs MOLMOL (17) and ProCheck (18).

Effect of Mutations in the Putative Fumarate Binding Site of DcuS on the Fumarate Plus DcuR-dependent Expression of dcuB′-′lacZ—The activity of the DcuS/DcuR two-component system was measured by the *dcuB′-′lacZ* reporter gene fusion. Expression of *dcuB* depends strongly on the presence of active DcuS/DcuR two-component system. Expression was measured after growth of the bacteria under anaerobic conditions ($A_{578\ nm} = 0.5$) with 50 mM fumarate as the substrates to achieve optimal induction of *dcuB*. All strains contain a chromosomal *dcuB′-′lacZ* reporter gene fusion. *E. coli* IMW260 is a derivative of *E. coli* K-12 with a chromosomal *dcuS* mutation (MC4100, but *dcuS*::*cam*^{R} *dcuB′-′lacZ*). The other strains were the same as IMW260, but contained various mutant forms of *dcuS* cloned in plasmid pET28a.

RESULTS AND DISCUSSION

Secondary Structure of DcuS-pd—The secondary structure of DcuS-pd (Fig. 1) consists of a long N-terminal α-helix (α_1) ranging from amino acid 46 to 64 with a continuation from 68 to 72 (α_2). After a short loop there is another α-helix (α_{3a}: 77–79) and (α_{3b}: 83–92) that is connected to the first β-strand (β_1: 97–102) of the four stranded antiparallel β-sheet. β_1 is connected via an α-helix (α_4: 126–128) and a long loop to the second β-strand (β_2: 134–138), which is connected by a short loop to the third strand (β_3: 145–153). Yet, another turn connects to the fourth β-strand (β_4: 159–167). From this strand the C-terminal helix follows after a short helix (α_5: 174–179). The secondary structural elements have been established by secondary chemical shifts as well as characteristic sequential NOEs and the connectivity of the four stranded antiparallel β-sheet by H^N,H_α and H_α,H_α cross-strand NOEs (Fig. 1). The secondary structure of DcuS including the transmembrane helices most probably is as follows: transmembrane helix 1 (21–42) to form a contiguous helix from 21 to 64. By the same token, it is expected that the C-terminal helix (α_5) extends into the membrane uninterruptedly via transmembrane helix 2 forming a helix from 174 to 202.

Structure Determination—The total number of non-am-

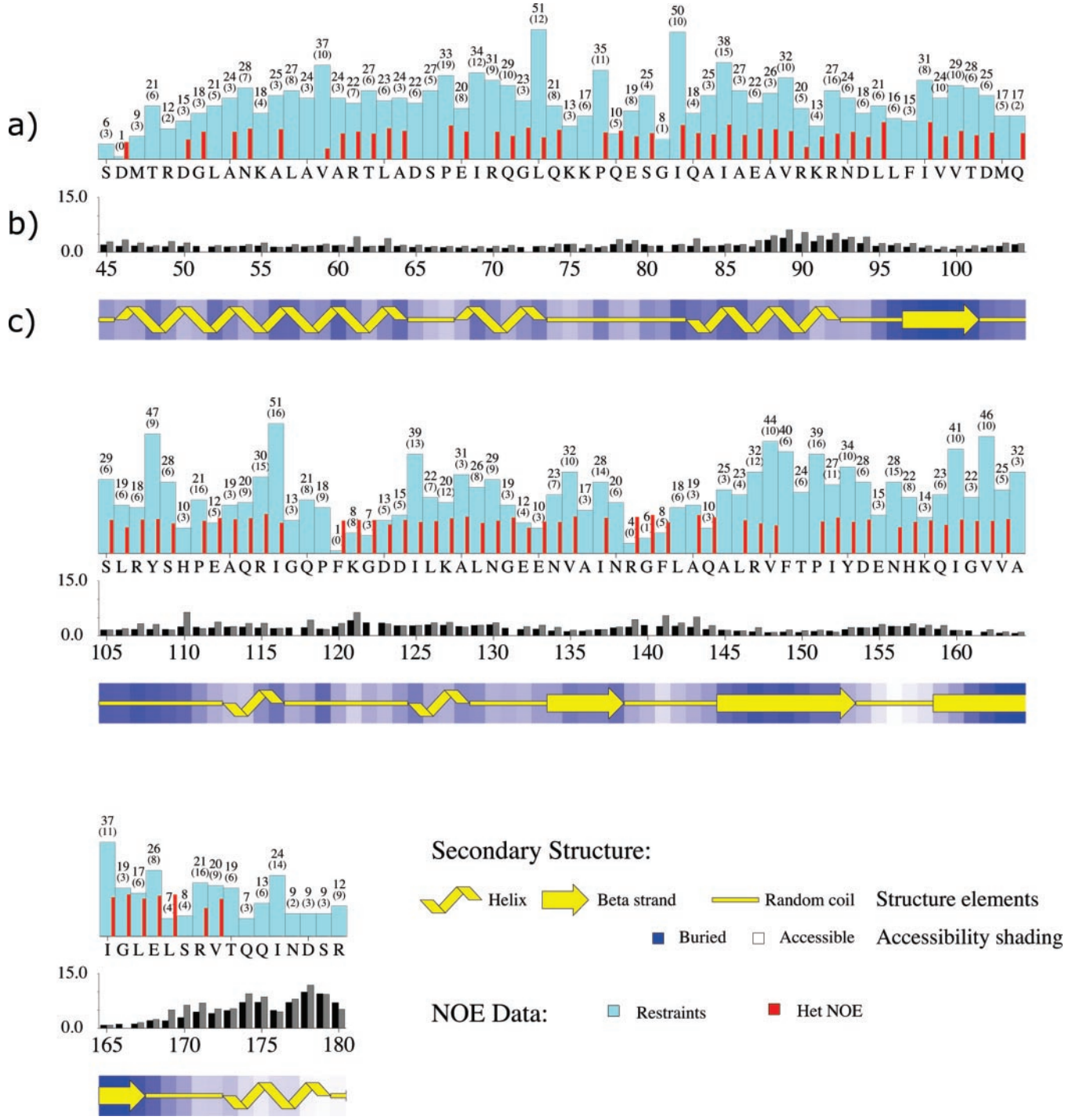

FIG. 2. **Statistics of number of NOE restraints, r.m.s.d. of the atomic positions, and secondary structure elements for DcuS.** The r.m.s.d. of each amino acid correlates very well with the number of restraints. This is expected since the heteronuclear NOE does not show appreciable variations across the structure of DcuS. *a*, numbers of restraints per residue, heteronuclear (*Het*) NOE value; *b*, r.m.s.d. from mean coordinates: main chain (*black*) and side chain (*gray*); *c*, secondary structure and average estimated accessibility.

biguos NOEs is 2245 (16.5 per residue) with 1074 (8 per residue) being inter-residual. We measured 382 dipolar couplings including 107 NH, 95 $H_\alpha C_\alpha$, 114 NC′, and 66 $C_\alpha C'$. 46 hydrogen bonds have been included as described above. 187 ϕ and ψ angles were derived from the carbon chemical shifts using Talos. $^1J(C_\alpha,H_\alpha)$ couplings were used to define the ϕ angle: negative for $^1J(C_\alpha,H_\alpha) > 137$ Hz and in the α-helix (19) range for $^1J(C_\alpha,H_\alpha) > 145$ Hz. Fig. 2 shows the distribution of NOEs and the resulting backbone r.m.s.d. as a function of sequence position. The backbone r.m.s.d. clearly anticorrelates with the number of NOE restraints per amino acid identifying several loops with reduced restraint density. Out of the 200 structures we took 10 structures that had the lowest energies and displayed them using the program MOLMOL (17). They had converged with an r.m.s.d. to the average structure of 0.68 Å in the backbone of the structured regions. The structure is well ordered in the region 46–168, while the first residues at the N terminus and the C-terminal residues (169–178) are not well ordered. Especially the C-terminal helix does not show long range NOEs.

Fig. 3 shows a stereo view of the mean structure derived from the 10 structures with the lowest energy, fitted for minimal

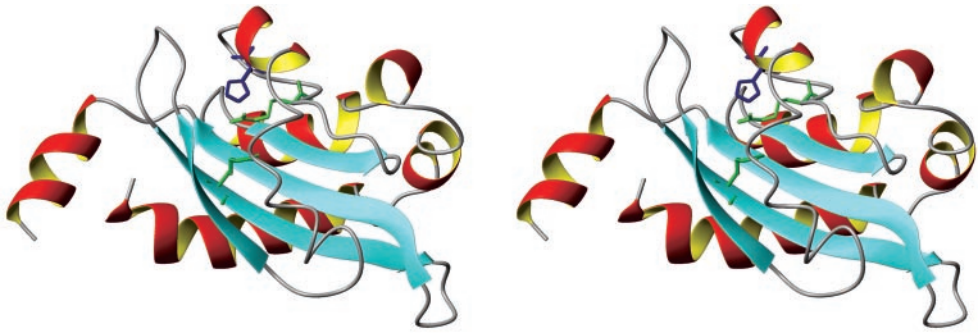

FIG. 3. **Stereo view of the structure of DcuS-pd indicating amino acids Arg^{107}, His^{110}, and Arg^{147}, which cluster together to form the putative binding site of fumarate.** The structure is a α,β-fold where both sides of the large β-sheet form hydrophobic cores with α-helices and the long connector between helix α_4 and strand β_2. The C-terminal helix is not fixed by NOEs and shows only small dipolar couplings, in agreement with a flexible helix.

TABLE I
Inactivation of DcuS in vivo by mutation of DcuS-pd

Strain (genotype)	β-Galactosidase	Wild-type/mutant activity
	Miller units	
IMW260 (*dcuS*$^-$)	7	0.033
IMW260 p(*dcuS*$^+$)	209	1
IMW260 p(*dcuS-R*107*A*)	6	0.029
IMW260 p(*dcuS-H*110*A*)	5	0.024
IMW260 p(*dcuS-R*147*A*)	11	0.053

r.m.s.d. (backbone rmsd 0.582, heavy r.m.s.d. 1.035) of the region with secondary structure elements (residues 55–88, 94–105, 123–136, 144–154, and 158–167). These structures were submitted to the Protein Data Bank as PDB ID 1ojg. The ^{1}N,^{15}N NOEs (Fig. 2) do not vary strongly over the structure of DcuS, except for the C-terminal helix.

Discussion of the Structure—The structure is a novel α,β-fold completely dissimilar of the four helix bundle structure of the aspartate sensor (20, 21). Also, the structure is a monomer in solution dissimilar to the aspartate sensor. From relaxation data the dimer content can be estimated to be below 10%, which is in agreement with gel shift data. In a DALI (22) search the closest match (score = 5) is photoactive yellow protein (PYP) from *Halorhodospirahalophila* (11), which also shows an α,β-fold, however, with 5 instead of 4 β-strands (Fig. 1). The topology of strands β_3, β_4, and β_5 of PYP is similar to the strands β_2, β_3, and β_4 of DcuS. However, the rest of the secondary structure is quite dissimilar. While in PYP the PAS core domain connects the strands β_2 and β_3 by crossing the whole β-sheet in a diagonal manner there is no PAS core domain in DcuS and the connection between sheets β_1 and β_2 is achieved on one side of the β-sheet. Similar to PYP, there are two hydrophobic cores on both sides of the β-sheet formed. Helices α_1 and α_{3b} bind to the bottom side of the β-sheet, while helix α_4 and the connector attach to the upper half of the β-sheet. In PYP the chromophore binding site is formed by the PAS core domain. Dissimilar to PYP, in DcuS residues located in the β-sheet (Arg^{147}) as well as in the connector (Arg^{107} and His^{110}) across the β-sheet contribute to the putative binding site of fumarate.

Relevance of the Structure—The periplasmic domain used in this study is folded and the residues Arg^{107}, His^{110}, and Arg^{147} found from mutation to be essential for fumarate binding are in close proximity in the structure, suggesting that the binding motif is retained in the periplasmic domain. Conservation of His and Arg residues in DcuS-pd, which have been assigned in citrate binding in CitA by mutagenesis (Table I), suggest that the same residues are important for fumarate binding in DcuS-pd. After mutagenesis of Arg^{107}, His^{110}, or Arg^{147} functional data were obtained by measuring the activity of the DcuS/DcuR two-component system via a *dcuB′-′lacZ* reporter gene fusion (Table I), the expression of which depends on the presence of active DcuS/DcuR two-component system (2). Replacement of the Arg residues 107 and 147 and of the His residue 110 by Ala by site-directed mutagenesis abolished the stimulation by fumarate to the same extent as complete deletion of the *dcuS* gene (Table I), although the mutated protein was formed at normal levels.

REFERENCES

1. Janausch, G., Zientz, E., Tran, Q. H., Kröger, A., and Unden, G. (2002) *Biochim. Biophys. Acta-Bioenergetics* **1553,** 39–56
2. Janausch, G., Garcia-Moreno, I., and Unden, G. (2002) *J. Biol. Chem.* **277,** 39809–39814
3. Parkinson, J. S., and Kofoid, E. C. (1992) *Annu. Rev. Genet.* **26,** 71–112
4. Zientz, E., Bongaerts, J., and Unden, G. (1998) *J. Bacteriol.* **180,** 5421–5425
5. Golby, P., Davies, S., Kelly, D. J., Guest, J. R., and Andrews, S. C. (1999) *J. Bacteriol.* **181,** 1238–1248
6. Kaspar, S., Perozzo, R., Reinelt, S., Meyer, M., Pfister, K., Scapozza, L., and Bott, M. (1999) *Mol. Microbiol.* **33,** 858–872
7. Parac, T. N., Coligaev, B., Zientz, E., Unden, G., Peti, W., and Griesinger, C. (2001) *J. Biomol. NMR* **19,** 91–92
8. Bartels, C., Xia, T. H., Billeter, M., Guntert, P., and Wüthrich, K. (1995) *J. Biomol. NMR* **6,** 1–10
9. Cornilescu, G., Delaglio, F., and Bax, A. (1999) *J. Biomol. NMR* **13,** 289–302
10. Zweckstetter, M., and Bax, A. (2001) *J. Biomol. NMR* **20,** 365–377
11. Borgstahl, G. E. O., Williams, D. R., and Getzoff, E. D. (1995) *Biochemistry* **34,** 6278–6287
12. Hansen, M. R., Rance, M., and Pardi, A. (1998) *J. Am. Chem. Soc.* **120,** 11210–11211
13. Chou, J. J., Delaglio, F., and Bax, A. (2000) *J. Biomol. NMR* **18,** 101–105
14. Chou, J. J., and Bax, A. (2001) *J. Am. Chem. Soc.* **123,** 3844–3845
15. Delaglio, F., Grzesiek, S., Vuister, G. W., Zhu, G., Pfeifer, J., and Bax, A. (1995) *J. Biomol. NMR* **6,** 277–293
16. Schwieters, C. D., Kuszewski, J. J., Tjandra, N., and Clore, G. M. (2003) *J. Magn. Reson.* **160,** 65–73
17. Koradi, R., Billeter, M., and Wüthrich, K. (1996) *J. Mol. Graphics* **14,** 29–32 and 51–55
18. Laskowski, R. A., MacArthur, M. W., Moss, D. S., and Thornton, J. M. (1993) *J. Appl. Crystallogr.* **26,** 283–291
19. Vuister, G. W., Delaglio, F., and Bax, A. (1992) *J. Am. Chem. Soc.* **114,** 9674–9675
20. Milburn, M. V., Prive, G. G., Milligan, D. L., Scott, W. G., Yeh, J., Jancarik, J., Koshland, D. E., and Kim, S. H. (1991) *Science* **254,** 1342–1347
21. Yeh, J. I., Biemann, H. P., Pandit, J., Koshland, D. E., and Kim, S. H. (1993) *J. Biol. Chem.* **268,** 9787–9792
22. Holm, L., and Sander, C. (1993) *J. Mol. Biol.* **233,** 123–138

Protein Structure and Folding:

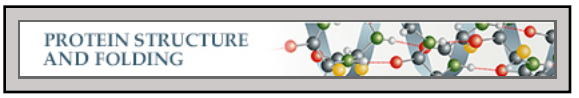

The NMR Structure of the Sensory Domain of the Membranous Two-component Fumarate Sensor (Histidine Protein Kinase) DcuS of *Escherichia coli*

Lucia Pappalardo, Ingo G. Janausch, Vinesh Vijayan, Eva Zientz, Jochen Junker, Wolfgang Peti, Markus Zweckstetter, Gottfried Unden and Christian Griesinger

J. Biol. Chem. 2003, 278:39185-39188.
doi: 10.1074/jbc.C300344200 originally published online August 7, 2003